EPRG-PRCI-APGA
23rd Joint Technical Meeting
Edinburgh, Scotland
6–10 June 2022

INCORPORATING STRAIN HARDENING AND THE 3D SHAPE OF METAL LOSS INTO CORROSION ASSESSMENT
PAPER NUMBER: 24

Bo Wang and Yong-Yi Wang*
Center for Reliable Energy Systems, Dublin OH, US

Brian Leis
B N Leis Consultant, Inc, Worthington OH, US

* Presenting author

ABSTRACT

A new burst pressure predictive model for isolated metal loss is presented. The new model incorporates two key features in comparison with existing models: (1) line-pipe's strain hardening rate represented by the strain hardening exponent $\boldsymbol{n}$ and (2) coupled effect of multiple parameters including circumferential width, planar shape, and longitudinal profile, in addition to the depth and axial length of a metal loss.

Multiple reference stress functions that incorporate the effects of pipe's UTS and strain hardening exponent $\boldsymbol{n}$ were examined for a wide range of pipe vintage and grades by performing numerical analysis, conducting full-scale burst tests of purposefully selected pipes with a wide range of strain hardening rates, and collecting additional full-scale test data. The Zhu-Leis reference stress function considered previously in work for PRCI is recommended for future use.

The coupled effect of width with metal loss planar shape and longitudinal profile is incorporated in the new model based upon an extensive finite element modeling of isolated metal loss. The model is evaluated against the existing full-scale burst tests. The effect of width on burst pressure was found to be dependent on the characteristics of the metal loss, such as the relative depth, planar geometry, and the length of the metal loss. The model is presented in a predictive equation coupled with look-up tables that account for the interacting effects of metal loss depth, axial length and profile, circumferential width, and planar shape.

The new model lays the foundation for the next phase work, i.e., extending the model to quantify the interaction and coalescence of adjacent metal-loss features. Upon completion, the model would help reducing unnecessary digs and rehabilitation while maintaining integrity and safety.

DISCLAIMER

1. Introduction

1.1. Background

The statistics on pipeline failures maintained in the United States (US) [1], Canada, Europe, and elsewhere indicate that corrosion anomalies remain a major threat to the integrity of natural gas and hazardous liquid pipelines. Integrity assessment of corrosion anomalies relies on two elements: (1) inspection to detect and size the metal loss anomalies and (2) the use of assessment models to predict the remaining strength (i.e., burst pressure) and the period of safe operation prior to reestablishing the pipeline's integrity. The work presented here focuses on the development of a new burst pressure predictive model for isolated metal loss funded under PRCI EC-2-10 project [2].

1.2. Existing Metal Loss Assessment Models

1.2.1. History of Model Development

Models to predict the burst pressure of metal loss have been developed and evolved since the late 1960s. About that time many of the pipelines that were constructed in the 1940s were being re-habilitated to deal with corrosion. Early assessment models heavily relied on full-scale test data as the basis to calibrate empirical fits to the test data. Such work led to ASME B31G [3] and Modified ASME B31G/RSTRENG [4]. RSTRENG was unique in that its application of Modified ASME B31G facilitated burst pressure predictions of complex corrosion features. Although these models were widely used by pipeline industry, their predicted burst pressures sometime were overly conservative as indicated by the NOVA's research around 1990 [5,6]. Those overly conservative predictions motivated a second wave of model development.

Because in-service corrosion had not yet been experienced for modern steels, the development of this new wave of models relied on numerical methods, like finite element analysis (FEA). Work by SHELL Global emerged early in this development cycle in the form of SHELL92 [7]. As its limitations were recognized by PCORRC [8] and DNV-RP-F101 [9], these models emerged in sequence as this second wave continued. As time passed the initial DNV model was later adapted for applications to complex-shaped metal loss.

For a pipe with metal loss, in addition to pipe geometry and pipe properties, the predicted burst pressure is reduced relative to its defect-free counterpart by the size and shape of the metal loss, and by the interaction and coalescence that can occur between adjacent metal-loss features. More recent work has been done to extend the predictive capabilities of the existing models to manage the scope of features identified in MFL and UT tool runs, and to better deal with the complexity that is emerging as those tools evolve. One of the most recent models is the Plausible Profile Model (Psqr) [10,11] which has been demonstrated to be safe, and more accurate and precise than RSTRENG for assessing large metal-loss corrosion based on ILI or field measurement. That said, the level of improvement in accuracy and precision of burst pressure prediction depends on the corrosion morphology.

1.2.2. General Format of Metal Loss Burst Pressure Predictive Models

Most of the exiting burst pressure predictive models of the corroded pipes typically coupled the response of defect-free pipes with a second multiplicative term that accounts for the effects of a metal loss. The burst pressure, P_b, is given as:

$$P_b = P_f \times f_{ML} \tag{1}$$

where P_f is the burst pressure of defect-free pipes and f_{ML} is a function of metal loss size and shape, which represents the burst pressure reduction due to a metal loss. P_f can be determined by a reference stress function and the pipe's geometry, see Section 2. The parameter f_{ML} can be generally

determined by two methods. One is to use the bulging factor, M, shape factor, α, and normalized metal loss depth, d/t, with the equation below:

$$f_{ML} = \frac{1 - \alpha \times (d/t)}{1 - \alpha \times (d/t) \times (M)^{-1}} \quad (2)$$

where the values of M and α depend on the specific assessment model [12]. Another method is to conduct the regression analysis on FEA results to get f_{ML} which is a function of normalized metal loss length and depth, see Eq. (3). This method has been used by Choi et al. [13] and in the R-PCORRC model[1] [14].

$$f_{ML} = f(L/(Dt), d/t) \quad (3)$$

where D is pipe outer diameter and L is metal loss length along the pipe longitudinal direction.

1.2.3. Limitations of Existing Assessment Models

Because of the complexity in full-scale experiments and in simulating complex corrosion most models have been developed relative to isolated rectangular flat-bottomed metal-loss features. For this reason, existing assessment models suffer two main limitations. The first is they do not account for the effects of pipe's strain hardening on burst pressure prediction. Although a few models such as R-PCORRC include the strain hardening exponent n, the application of these models was limited due to the insufficient validation (i.e., they were validated over a narrow range of strain hardening rates).

The second limitation is that they do not account for the effect of metal loss width in burst pressure prediction, nor do they consider the planar shape of the feature or its longitudinal profile. It is well known that the extent of metal loss along the pipe longitudinal direction is more important than the circumferential width as the hoop stress in most pipe segments is typically greater than longitudinal stress. Most of the existing models use a single simple corrosion geometry in the pipe longitudinal direction and the corrosion circumferential width is not considered. However, some recent studies [14-18] have indicated that, in addition to metal loss longitudinal length and depth, the metal loss circumferential width, planar shape, and longitudinal profile also affect the burst pressure of isolated metal loss.

1.3. Scope of This Paper

This paper covers the development and evaluation of a new burst pressure predictive model for isolated metal loss and includes two parts: (1) a reference stress function which incorporates the effects of both pipe UTS and strain hardening rate and (2) a corrosion assessment model which incorporates metal loss 3D shape by including coupled effects among circumferential width, planar shape, and longitudinal profile, in addition to the depth and axial length of a metal loss.

2. Reference stress function

The reference stress is the failure stress of defect-free pipes under internal pressure. The burst pressure of defect-free pipes can be determined by the reference stress function, σ_R, and a function of pipe's dimension (i.e., D and t), f_{pipe}, via the equation below:

$$P_f = \sigma_R \times f_{pipe} \quad (4)$$

Since the reference stress function of 1.1 times SMYS used by ASME B31G, many different functions of reference stress have been adopted over the years [19]. There are three major types of reference stress functions:

(1) SMYS based, e.g., 1.1 SMYS in ASME B31G or SMYS (in ksi) + 10 ksi in Modified ASME B31G;
(2) SMTS based, e.g., SMTS in DNV model or 0.9 SMTS in SHELL92 model; and

[1] The original PCORRC model was reformulated and named R-PCORRC, see [14].

(3) Pipe UTS[2] σ_{UTS} and strain hardening exponent n based.

Various UTS and □ based reference stress functions reviewed in this work are given below:

$$\sigma_{R,M} = 2\left(\frac{1}{\sqrt{3}}\right)^{n+1}\sigma_{UTS} \quad (5)$$

$$\sigma_{R,T} = 2\left(\frac{1}{2}\right)^{n+1}\sigma_{UTS} \quad (6)$$

$$\sigma_{R,ZL} = 2\left(\frac{2+\sqrt{3}}{4\sqrt{3}}\right)^{n+1}\sigma_{UTS} \quad (7)$$

$$\sigma_{R,EC-2-6} = (1.0745 - 0.6131n)\sigma_{UTS} \quad (8)$$

$$\sigma_{R,EC-2-10} = \left(\frac{2}{\sqrt{3}}\right)(0.933)^{(n+1)}(1.000 - 0.520n)\sigma_{UTS} \quad (9)$$

Eq. (5) and Eq. (6) are based on von Mises and Tresca equivalence criteria, respectively. Eq. (7) was obtained from a new equivalence criterion called average shear-stress criterion or Zhu-Leis criterion [20]. The reference stress functions from PRCI project EC-2-6 [23] and the current project EC-2-10 [2] are given in Eq. (8) and Eq. (9).

One of the main objectives of the current work was to examine the applicability of the newly developed reference stress functions, such as Zhu-Leis, EC-2-6, and EC-2-10 for a wider range of pipe vintage and grades than past work by performing numerical analysis, conducting full-scale burst tests of purposefully selected pipes with a wide range of strain hardening rates, and collecting additional full-scale test data [2]. The evaluation of these reference stress functions are briefly summarized below.

Figure 2-1 shows the normalized failure pressures from the tests and prediction via different reference stress functions. P_o in Y-axis is determined by $(2t/(D-t))\sigma_{UTS}$. "Measured n" on the X-axis is obtained from experimentally measured full stress-strain curves using the standard procedures of determining n in ASTM E646-16 [21].

Figure 2-1 has two groups of data:

- Group 1: The measured burst pressures from the full-scale burst tests. These data are shown by the individual symbols. There are 37 full-scale test data sets which include: (1) 5 from EC-2-10 [2]; (2) 13 from EC-2-6 [22,23]; and (3) 19 from past test archival database and literatures [24-27].

- Group 2: The predicted burst pressures using the reference stress functions of von Mises, Tresca, Zhu-Leis, EC-2-6, and EC-2-10. These data are shown in solid lines.

It can be concluded from Figure 2-1 that:

(1) The burst pressure data shows a decreasing trend with respect to n.
(2) The von Mises reference stress function lies above the test data, whereas the Tresca reference stress function falls below the test data.

[2] Here pipe UTS can be either SMTS or actual UTS measured from tensile tests.

(3) The reference stress functions of Zhu-Leis, EC-2-6, and EC-2-10 are essentially the same and they all run through the middle of the full-scale burst test data. On the average, they provide a good agreement with the test data.
(4) The present work provides an independent, robust, and broad validation of the EC-2-6 and Zhu-Leis reference stress functions.
(5) Given the more robust development process and demonstrated broad applicability from this work, the Zhu-Leis reference stress function is recommended for future use.

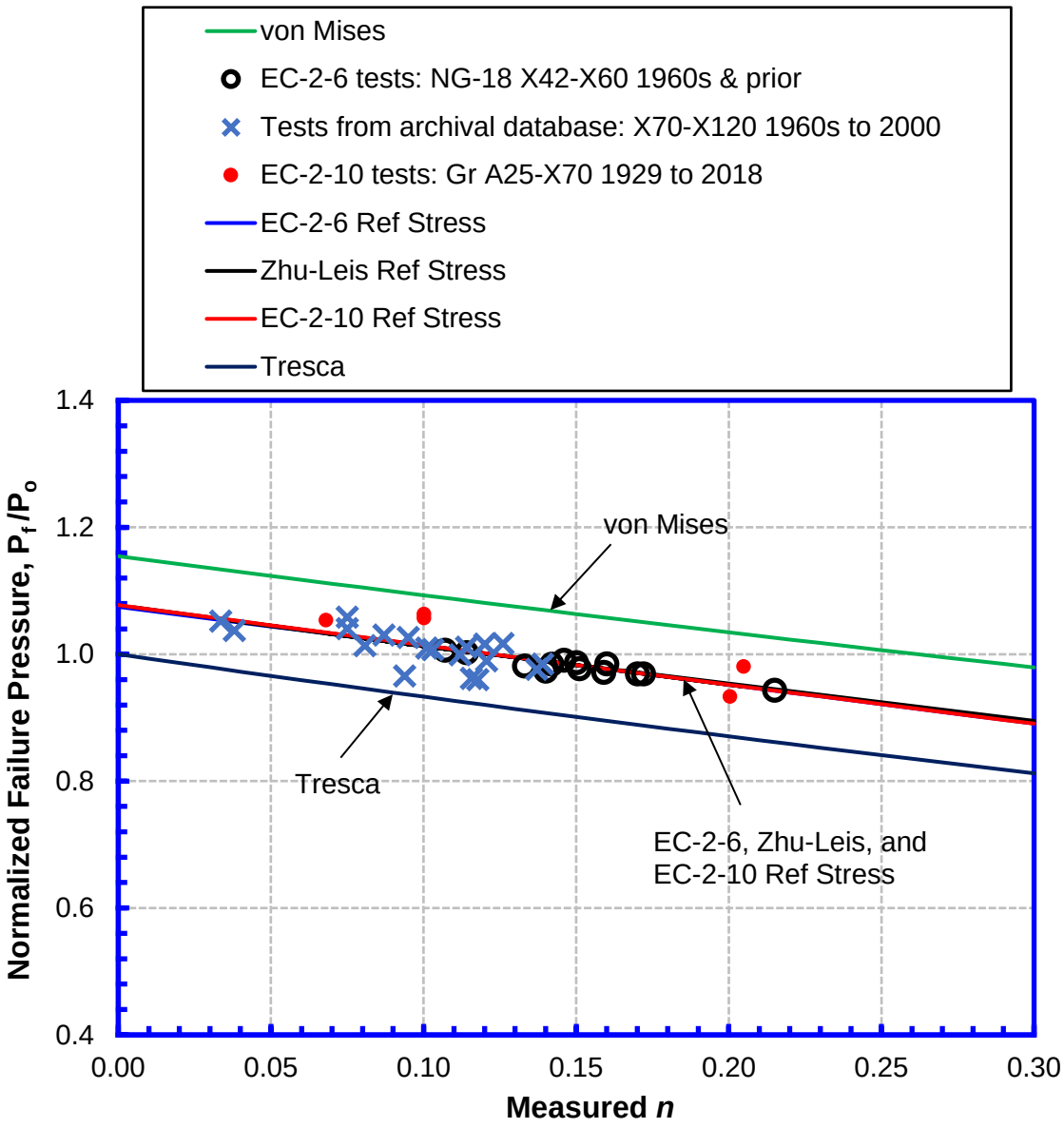

Figure 2-1 Normalized failure pressures vs. strain hardening exponent from the full-scale burst tests and different reference stress functions

3. Burst pressure predictive model of isolated Metal Loss

3.1. Analysis Approach and Steps

The overall approach in developing the predictive model includes: (1) numerically simulating the burst pressure for pipes containing a variety of metal-loss geometries; and (2) organizing and trending the data as the basis to develop a predictive model. Thereafter, the model is evaluated against available test data. The process involves the following steps:

(1) Step 1: Perform 2-D and 3-D FEA to develop trends for variation of burst pressure with respect to length, depth, and width of isolated metal loss with rectangular planar shape and flat-bottomed longitudinal profile (see Figure 3-1).
(2) Step 2: Develop a burst pressure predictive model for rectangular flat-bottomed metal loss.
(3) Step 3: Evaluate the developed model from Step 2 against existing full-scale burst test data.
(4) Step 4: Conduct 3-D FEA to predict the burst pressure of isolated metal loss with elliptical planar shape and parabolic longitudinal profile (thereafter, named elliptical parabolic metal loss) (see Figure 3-2).
(5) Step 5: Extend the model from Step 2 to consider elliptical parabolic metal loss.

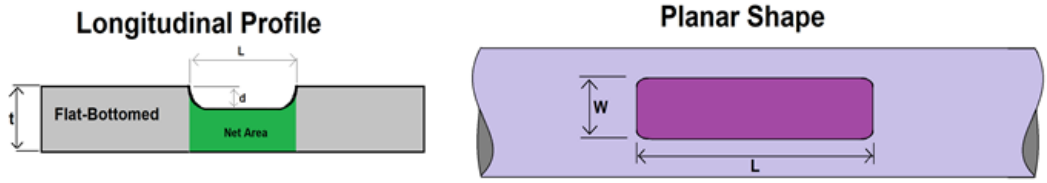

Figure 3-1 Schematic of a rectangular flat-bottomed metal-loss feature

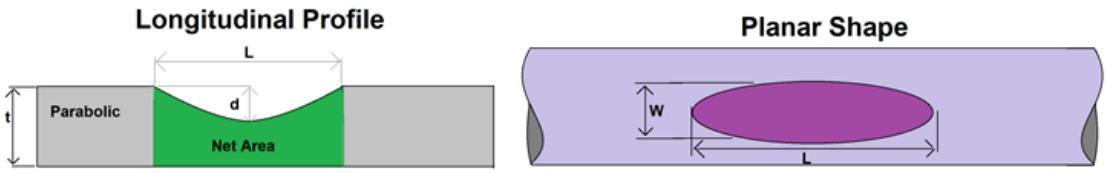

Figure 3-2 Schematic of an elliptical parabolic metal-loss feature

The circumferential profiles of the above two shapes are shown in Figure 3-3. The depth remains constant in the circumferential direction for a rectangular flat-bottomed feature, whereas for an elliptical parabolic feature the depth smoothly changes from maximum at the center to zero at the edges following a parabolic pattern.

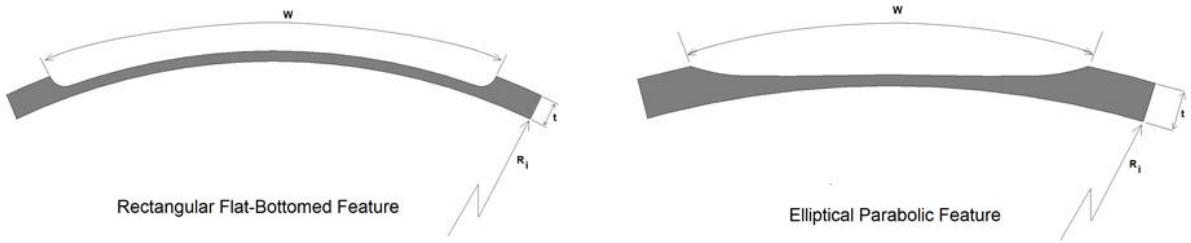

Figure 3-3 Schematic of circumferential profile of a rectangular flat-bottomed metal-loss feature (left) and an elliptical parabolic metal-loss feature (right)

3.2. FE Models

All FE models of a pipe with isolated metal loss were generated and solved using ABAQUS. For 3-D FEA, ABAQUS 20-node continuum brick element (C3D20R) was used. Mesh convergence study suggested the use of minimum 7 layers of elements through the pipe wall thickness in metal loss region. Due to symmetry, only a quarter of a pipe was modeled with appropriate symmetric boundary conditions, see Figure 3-4.

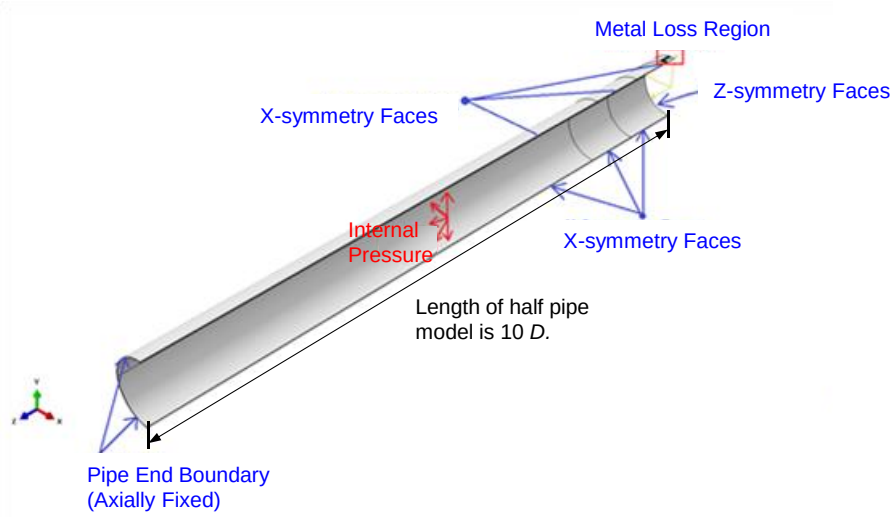

Figure 3-4 Schematic of FE model of a pipe with rectangular flat-bottomed metal loss

For each FEA case, the pipe internal pressure was incrementally increased from zero up to the point where the pipe was not capable of withstanding any additional internal pressure. ABAQUS built-in automatic time stepping algorithm, based on the modified arc-length technique (RIKS method), was used to increment the load. The maximum achieved internal pressure was identified as the corresponding pipe burst pressure.

3.3. Effects of Metal Loss Width

The effects of metal loss width on burst pressure prediction were examined through FEA of a pipe with metal loss of various lengths, depths, widths, and shapes. The outcomes of the FEA follow:

(1) In Section 3.3.1, for rectangular flat-bottomed metal loss, the predicted burst pressure and plastic strain contour from FEA cases with different metal loss width are shown and the effects of metal loss width on burst location and burst pressure are discussed.
(2) In Section 3.3.2, for elliptical parabolic metal loss, the effects of metal loss width on the predicted burst pressure are shown and discussed.

3.3.1. Effects of Width for Rectangular Flat-Bottomed Metal Loss

Four cases with the same metal loss length and depth, but different metal loss width angle from 5 to 60 degrees were analyzed. The pipe geometry, pipe material properties, and metal loss sizes of these 4 cases are summarized in Table 3-1. Here ⍰⍰ is the arc length of metal loss width along the pipe circumference.

Table 3-1 Pipe geometry and material, metal loss sizes analyzed and FEA predicted burst pressures

Case #	Pipe Geometry and Material				Metal Loss Depth, Length, and Width						FEA Predicted Burst Pressure
	D	*t*	UTS (ksi)	*n*	*d*/*t*	$L/\sqrt{Dt}$	*L* (in)	*W* (Deg)	*W*c (in)	Aspect Ratio *W*c/*L*	
1	36	0.5	100	0.07	0.8	0.5	2.1	5	1.6	0.7	2957
2								30	9.4	4.4	2925
3								45	14.1	6.7	2835
4								60	18.8	8.9	2754

Figure 3-5 shows the equivalent plastic strain (i.e., PEEQ) contour from FEA when the pipe reached the highest pressure (i.e., burst pressure) for these 4 cases. The grey area within the

metal-loss feature indicates the region where the plastic strain is higher than the defined maximum value (i.e., 0.6) and also indicates the burst location. The predicted burst pressures corresponding to these 4 cases are also summarized in last column of Table 3-1.

For Case 1 in Figure 3-5, the metal loss width is small and the burst location is about halfway between the center and Edge 1. When the width is increased, the burst location shifts from the center towards Edge 1 in Case 2 and Case 3. When the width is further increased from 45 to 60 degrees in Case 4, the burst location shifts from Edge 1 to Edge 2. From the last column of Table 3-1, the predicted burst pressure decreases with the increase of metal loss width angle.

The bulging at the metal loss area increases with the increase of metal loss width, which increases the local bending such that the burst location shifts from the center location dominated by membrane stress to the edge of metal loss where local bending combines with membrane stress. The predicted burst pressure decreases with the increase of width due to the combined local bending and membrane stresses. When the metal loss circumferential width is increased, the pipe longitudinal stress is increased due to increased metal loss which could shift burst location from Edge 1 to Edge 2.

The effect of metal loss width can also be seen in Figure 3-6. For the short and deep rectangular flat-bottomed metal loss shown in blue solid line with square symbol, increasing width angle results in decreasing burst pressure. For the relatively long and shallow rectangular flat-bottomed metal loss shown in red dash line with triangular symbol, the effect of metal loss width is marginal on burst pressure.

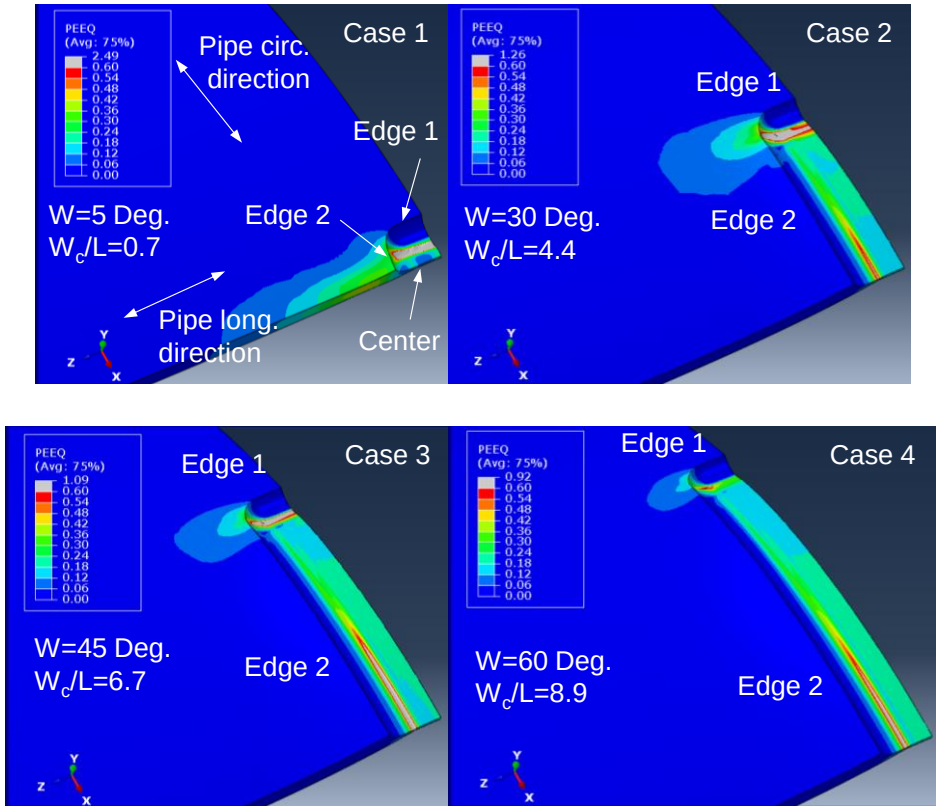

Figure 3-5 PEEQ contour of rectangular flat-bottomed metal loss with different widths from FEA

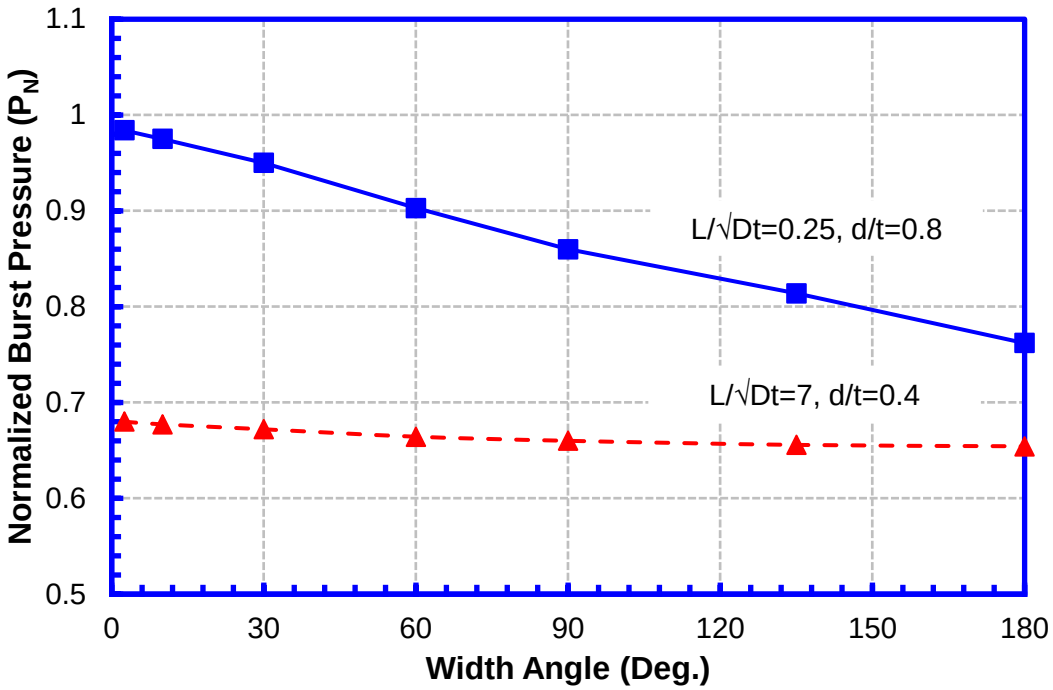

Figure 3-6 Variation of P_N with width angle of rectangular flat-bottomed metal loss for the pipe of 36" OD and 0.5" WT with UTS = 100 ksi and strain hardening exponent = 0.07

3.3.2. Effects of Width for Elliptical Parabolic Metal Loss

The burst pressure of a pipe with elliptical parabolic metal loss was analyzed for different combination of metal loss length, depth, and width. Here, two cases with the same metal loss depth and different length and width are presented. The pipe OD is 36" and WT is 0.5" with pipe UTS of 100 ksi and strain hardening exponent n of 0.07. The normalized metal loss depth d/t is 0.4. The normalized metal loss length $L/\sqrt{Dt}$ is equal to 1 and 4. The metal loss width angle is increased from 0 to 90 degrees.

As shown in Figure 3-7, for both short and relatively long metal-loss features with elliptical parabolic shape, increasing the width angle results in increasing the pipe burst pressure. This trend was also found in the work of [17,18] which indicates that increasing width angle can be beneficial for burst pressure.

The above observation is counterintuitive compared to the rectangular flat-bottomed shape trend depicted in Figure 3-6. For an elliptical parabolic metal-loss feature, a smooth transition from the deepest point of the feature at the center to the edges of the feature exists, see Figure 3-3. This transition becomes smoother with increasing width angle in the pipe circumferential direction. As a result, increasing the width angle results in a transition from the combined membrane and bending deformation for narrow features to a membrane dominated deformation for wide features.

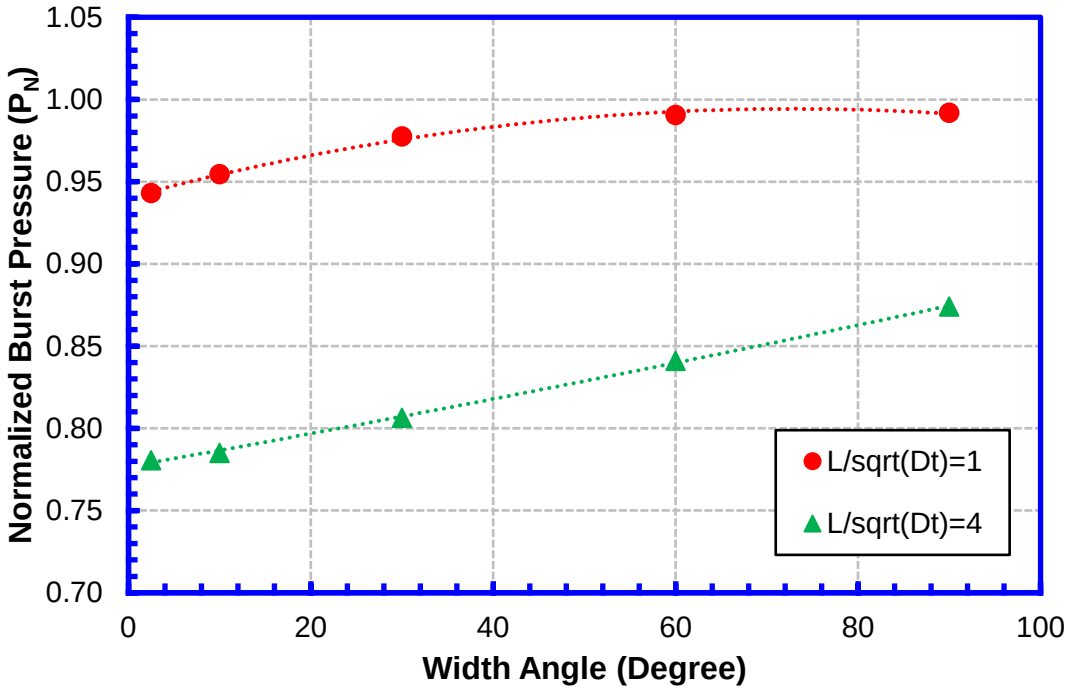

Figure 3-7 Variation of P_N with width angle of elliptical parabolic metal loss ($d/t = 0.4$) for the pipe of 36" OD and 0.5" WT with UTS = 100 ksi and strain hardening exponent = 0.07

3.4. Burst Pressure Predictive Model

A burst pressure predictive model for isolate metal loss with rectangular flat-bottomed shape was developed based on trending the normalized burst pressure values from the FEA. The model is given by Eq. (10) and Eq. (11):

$$P_N = \frac{(1 - d/t)}{1 - (d/t) \times F\left(L/\sqrt{Dt}, W\right)} \tag{10}$$

$$P_b = P_N \times \sigma_{R,ZL} \times (2t/D) \tag{11}$$

where F is a function of $L/\sqrt{Dt}$ and W which includes the effect of metal loss length and width. This function is given in a look-up table, see Table A-1 in Appendix A. The range of validity of Eq. (10) and Eq. (11) is as follows:

- Normalized depth: $0.1 \leq d/t \leq 0.9$,
- Normalized length: $0.25 \leq L/\sqrt{Dt} \leq 10$, and
- Width angle: $2.5 \leq W \leq 180$ degrees.

3.5. Evaluation of Burst Pressure Predictive Model

3.5.1. Comparison to FEA and Other Model Predictions

The comparison of P_N predicted from EC-2-10 Eq. (10) vs. that from FEA is shown in Figure 3-8 and Figure 3-9 with respect to normalized metal loss length and depth, and selected width angles. A reasonably good agreement was obtained in P_N between the EC-2-10 model prediction and FEA results for all examined cases.

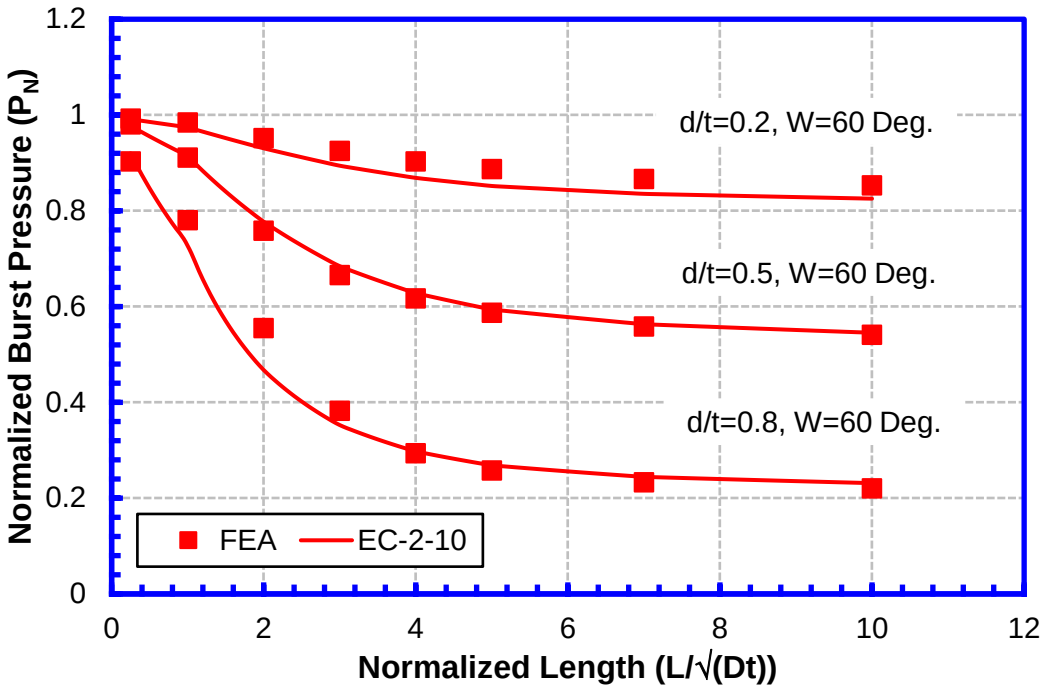

Figure 3-8 Comparison of P_N vs. metal loss length from FEA and EC-2-10 model

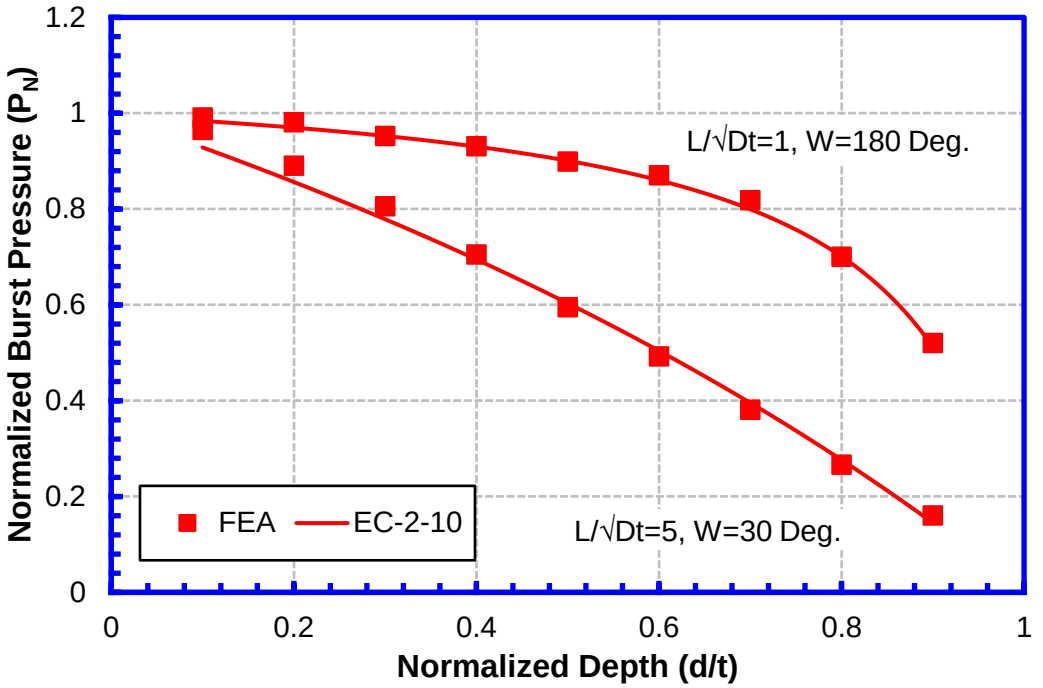

Figure 3-9 Comparison of P_N vs. metal loss depth from FEA and EC-2-10 model

Figure 3-10 shows the comparison of P_N predicted from EC-2-10 Eq. (10), DNV, and R-PCORRC models vs. that from FEA with respect to metal loss width angle and selected metal loss length and depth. It can be seen from Figure 3-10 that, for the short and deep rectangular flat-bottomed metal loss, the present model is able to capture the effect of metal loss width angle on P_N. However, the DNV and R-PCORRC models cannot capture such effect. When the width angle is smaller than 30 degrees, the P_N from both the DNV and R-PCORRC models is lower than that from the present model. When the width angle is increased to between 30 and 70 degrees, the [illegible] from the present model is lower than that from the DNV model but higher than that from the R-PCORRC model. When the width angle is further increased to

between 70 and 180 degrees, the P_N from the present model is lower than that from either the DNV or R-PCORRC model.

The results shown in bottom of Figure 3-10 (i.e., for $L/\sqrt{Dt} = 7$ and $d/t = 0.4$) indicate that, for the relatively long and shallow rectangular flat-bottomed metal loss, the effect of metal loss width angle on P_N is marginal and the P_N from these three predictive models and FEA are very similar.

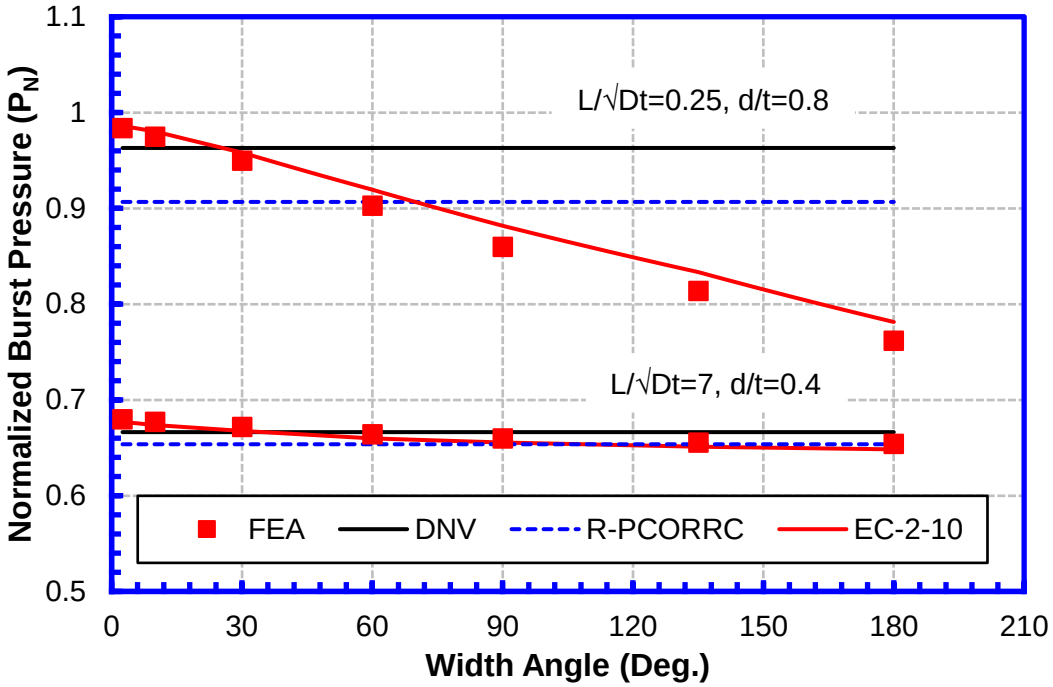

Figure 3-10 Comparison of P_N vs. metal loss width angle from FEA and various predictive models

3.5.2. Comparison to Existing Full-Scale Test Data

The burst pressure predictive model given in Eq. (10) and Eq. (11) was evaluated against a set of available full-scale burst test data developed for rectangular flat-bottomed metal-loss features machined into pipes [28-34]. There are 67 tests in total, which cover pipe grade from X52 to X80 and different pipe geometry and metal loss size, see Table 3-2. In addition to pipe grade, the actual YS and UTS were available.

The burst pressures of these 67 tests were predicted using Eq. (10) and Eq. (11) and the reported pipe D and t, the actual UTS, and the size of the metal loss. The strain hardening exponent n was determined using the equation below [14]:

$$n = -0.211 \times [AYS/SMYS - 1.2847 \times SMYS/(SMYS - 12.0655)] \quad (12)$$

where AYS is actual YS in ksi.

The burst pressure P_b from Eq. (11) was used to calculate the burst pressure ratio using the following equation:

$$P_{pre}/P_{exp} = P_b/P_{exp} \quad (13)$$

where P_{pre} and P_{exp} are predicted and measured burst pressures.

Figure 3-11 shows the unity plot between the predicted and measured burst pressures. Table 3-3 shows a comparison in burst pressure ratio in terms of the mean value, standard

deviation (Std), and coefficient of variation (CoV) among the present model and the ASME B31G, Modified ASME B31G, DNV, and R-PCORRC models.

It is evident that the present model improved the burst pressure prediction compared to ASME B31G and Modified ASME B31G, and resulted in burst pressure predictions similar to those from using the DNV and R-PCORRC models. Similar predictions for the newly developed model and those of DNV and R-PCORRC reflects the observation that the available full-scale test data is limited in regard to the effect of width. The test pipes do not include metal-loss features whose size and shape can reflect the effect of width. The next phase of this work will develop full-scale test results for metal-loss features designed to discriminate between these models, and empirically quantify width effects.

Table 3-2 Pipe geometry and metal loss sizes of the existing full-scale test data

Range of Parameters	Pipe Geometry			Metal Loss Length, Depth, and Width					
	D	t	D/t	L	$L/\sqrt{Dt}$	d	d/t	W_c	W
	mm	mm		mm		mm		mm	Deg.
Min.	219.2	8.1	8.6	40.0	0.66	3.7	0.20	18.8	3.9
Max.	917.4	25.4	69.1	2000.0	13.95	18.7	0.80	600.0	111.1
Median	612.1	18.7	41.5	342.9	3.19	10.9	0.70	100.0	16.8

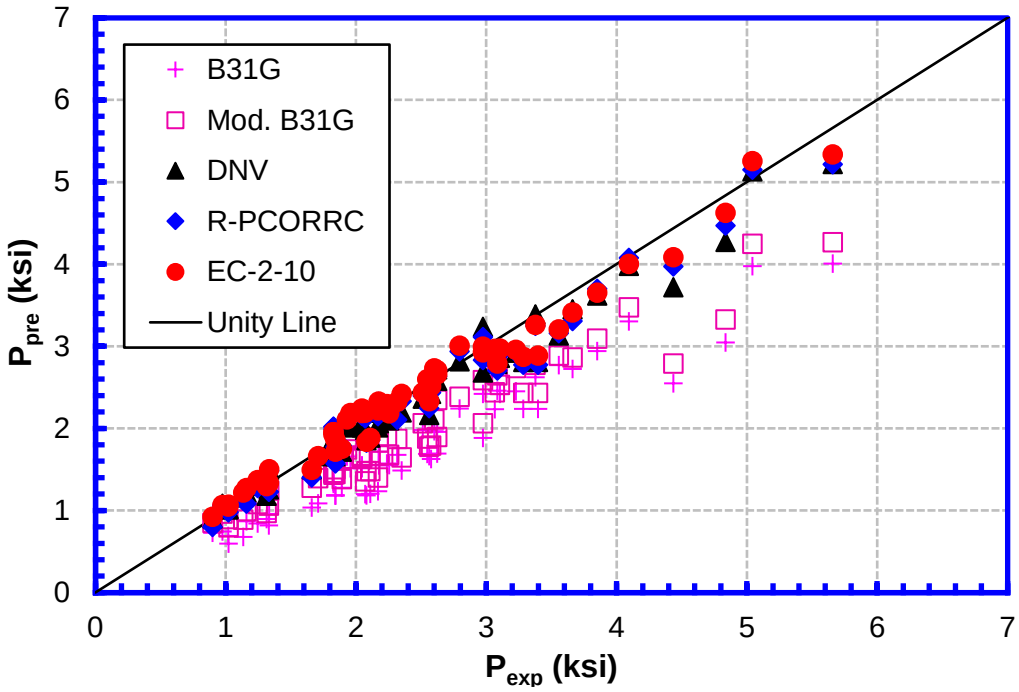

Figure 3-11 Unity plot of predicted and measured burst pressures

Table 3-3 Comparison of burst pressure ratio among different predictive models

Predictive Model	P_{pre}/P_{exp}				
	ASME B31G	Mod. B31G	DNV	R-PCORRC	EC-2-10
Mean	0.69	0.78	0.97	0.97	0.99
Std	0.09	0.09	0.07	0.08	0.07
CoV	0.12	0.11	0.07	0.08	0.08

3.6. Extension of the Model to Elliptical Parabolic Metal Loss

To extend the applicability of Eq. (10) and Eq. (11) to other metal-loss shapes, a shape effect factor $\boldsymbol{\lambda}$ was introduced below:

$$P_b^{EP} = \lambda\left(L/\sqrt{Dt}, d/t, W\right) \times P_b^{Rec} \quad (14)$$

where P_b^{EP} and P_b^{Rec} are the predicted burst pressures of elliptical parabolic and rectangular flat-bottomed metal-loss features, respectively. The ratio of P_b^{EP} to P_b^{Rec} was calculated for each case from FEA (i.e., for each combination of the selected $L/\sqrt{Dt}$, d/t, and W values). This defines a shape effect factor $\boldsymbol{\lambda}$ as a function of the metal loss length, depth, and width which converts the burst pressure of a rectangular flat-bottomed metal-loss feature to the burst pressure of an elliptical parabolic metal-loss feature with the same dimension. These analysis results led to a series of look-up tables which were summarized in Appendix E of PRCI EC-2-10 Phase 1 report [2].

4. Conclusions

A new burst pressure predictive model for isolated metal loss, i.e., EC-2-10 model, was developed. The following key findings have been observed:

(1) The model captures the coupled effects of metal loss width along with its planar shape, longitudianl profile, length, and depth, and can be applied to isolated metal loss with a wide range of metal loss sizes, planar shapes, and longitudinal profiles.
(2) The effects of width on burst pressure depend on the metal loss depth, length, planar shape, and longtiudinal profile.
(3) The evaluation against available full-scale test data showed that the EC-2-10 model provided improved burst pressure prediction compared to ASME B31G and Modified ASME B31G, and showed similar accuracy and precision compared to the DNV and R-PCORRC models. The similarity in the accuracy of prediction between the EC-2-10 model and the DNV and R-PCORRC models reflects limitations in the available full-scale burst tests which do not include metal-loss features whose size, planar shape, and longitudinal profile can differentiate the effect of width.
(4) More validation against the full-scale tests is needed to demonstrate the EC-2-10 model's capability of counting the effects of metal loss width. Such full-scale tests must be designed to discriminate the role of width. Work is planned to complete full-scale tests to bridge this gap.

The next phase of this work will use this model to quantify interaction and coalescence between adjacent features as the basis to extent its use for applications involving complex/real corrosion.

5. Acknowledgements

The financial support of PRCI is gratefully appreciated. The authors wish to acknowledge the contributions of Amin Eshraghi, PhD., P.Eng, to this work while he was on the staff of CRES.

6. References

1. https://primis.phmsa.dot.gov/comm/FactSheets/FSCorrosion.htm.
2. Wang, B., Eshraghi, A., Wang, Y.-Y., Leis, B., 2022, "Development of Comprehensive Metal Loss Assessment Methodologies," PRCI EC-2-10 Phase 1 report, Catalog No. PR350-203605-R01.
3. ASME B31G-2012 (Revision of ASME B31G-2009), 2012, "Manual for determining the remaining strength of corroded pipelines - Supplement to ASME B31 Code for Pressure Piping," The American Society of Mechanical Engineers, New York.
4. Kiefner, J. F. and Vieth, P. H., 1989, "A modified criterion for evaluating the remaining strength of corroded pipe, Final report on PR 3-805 to Pipeline Corrosion Supervisory Committee of the Pipeline Research Committee of the American Gas Association," Battelle, Ohio.
5. Coulson, K. E. W. and Worthingham, R. G., 1990, "Standard Damage-Assessment Approach is Overly Conservative," Oil & Gas Journal, Vol. 88, No. 15, pp. 54-59, April 9, 1990.
6. Coulson, K. E. W. and Worthingham, R. G., 1990, "New Guidelines Promise More Accurate Damage Assessment," Oil and Gas Journal, Vol. 88, No. 16, pp. 41-44, April 16, 1990.
7. Ritchie, D. and Last, S., 1995, "Burst criteria of corroded pipelines – defect acceptance criteria," Proceedings of EPRG/PRC 10th Biennial Joint Technical Meeting on Line pipe Research, 18-21 April 1995, Cambridge, UK, paper No.32.
8. Stephens, D. R., Leis, B. N., Kurre, M. D., and Rudland, D. L., 1999, "Development of an alternative failure criterion for residual strength of corrosion defects in moderate- to high-toughness pipe," Final report on PR 3-9509 to Line Pipe Research Supervisory Committee, PRC International, Virginia.
9. DNVGL-RP-F101, 2019 Edition, September 2019, "Corroded Pipelines," DET NORSKE VERITAS.
10. Zhang, S., Yan, J., Kariyawasam, S., Huang, T., and Al-Amin, M., 2018, "A More Accurate and Precise Method for Large Metal Loss Corrosion Assessment," IPC2018-78233, Proceedings of the 2018 12th International Pipeline Conference, September 24-28, 2018, Calgary, Alberta, Canada.
11. Zhang, S., Yan, J., Kariyawasam, S., Huang, T., and Al-Amin, M., 2020, "Plausible Profile (Psqr) Corrosion Assessment Model: Refinement, Validation and Operationalization," IPC2020-9448, Proceedings of the 2020 13th International Pipeline Conference, September 28-30, 2020, Virtual, online.
12. Chauhan, V. and Brister, J., 2009, "A Review of Methods for Assessing the Remaining Strength of Corroded Pipelines," Report for USDOT PHMSA DTPH56-05-T0003 - Project 153, Report #:6781, prepared by GL Industrial Services UK Ltd.
13. Choi, J.B., Goo, B.K., Kim, J.C., Kim, Y.J. and Kim, W.S., 2003, "Development of limit load solutions for corroded gas pipelines," International Journal of Pressure Vessels and Piping, 80(2):121 – 128.
14. Leis, B. N., 2021, "Evolution of metal-loss severity criteria: Gaps and a path forward," Journal of Pipeline Science and Engineering 1 (2021) 51–62.
15. Leis, B.N., Zhu, X.-K., and McGaughy, T., 2016, "Assessment of Corrosion Model Error for Metal-Loss Defects in Pipelines," Phase I Report of PRCI Project EC-2-7, Catalog No. PR-185-143600-R01.
16. Leis, B.N., 2020, "Continuing Development of Metal-Loss Severity Criteria, including Width Effects," IPC2020-9575, Proceedings of the 2020 ASME International Pipeline Conference, September 28 - October 02, 2020; Calgary, AB, Canada.
17. Zhang, S. and Zhou, W., 2020, "Assessment of effects of idealized defect shape and width on the burst capacity of corroded pipelines," Thin-Walled Structures 154 (2020) 106806.
18. Zhang, S. and Zhou, W., 2021, "Development of a burst capacity model for corroded pipelines considering corrosion defect width and a revised Folias factor equation," Journal of Natural Gas Science and Engineering, Volume 88, April 2021, 103812.
19. Zhu, X.-K., 2021, "A comparative study of burst failure models for assessing remaining strength of corroded pipelines," Journal of Pipeline Science and Engineering 1 (2021) 36–50.

20. Zhu, X.-K. and Leis, B. N., 2006, “Average shear stress yield criterion and its application to plastic collapse analysis of pipelines,” International Journal of Pressure Vessels and Piping 83 (2006) 663–671.
21. ASTM E646-16, 2016, “Standard Test Method for Tensile Strain-Hardening Exponents (n - Values) of Metallic Sheet Materials,” ASTM International.
22. NG-18 archive Battelle, provided by Brian Leis.
23. Zhu, X.-K., Leis, B.N., and McGaughy, T., 2018, “Reference Stress for Metal-loss Assessment of Pipelines,” Final report of PRCI EC-2-6, Catalog No. PR-185-173600-R01.
24. Operator supplied-data, provided by Brian Leis.
25. Knoop F.M., Flaxa, V., Zimmermann, S., and Groß-Weege, J., 2010, “Mechanical Properties and Component Behavior of X80 Helical Seam Welded Large Diameter Pipes,” IPC2010-31602, Proceedings of the 2010 8th International Pipeline Conference, September 27-October 1, 2010, Calgary, Alberta, Canada.
26. Papka, S.D., 2003, “Full Size Testing and Analysis,” 13th International Offshore and Po-lar Engineering Conference (ISOPE-2003), Honolulu, Hawaii, USA, May 25-30, 2003.
27. Amano K., Matsuoka M., Ishihara T., Tanaka K., Inoue T., Kawaguchi Y., and Tsukamoto M., 1986, “Significance of yield ratio limitation to plastic deformation of pipeline in high pressure proof test,” 7th Symposium on Line Pipe Research, Houston, October, 1986; pp. 8.1-8.21.
28. BG test data, GRTC R1803, R1804 and R1805, 1997.
29. Lefevre, T., 2007, “Summary Report on Full-Scale Burst Testing of 24-inch by 10.3 mm Steel Pipes of API 5L X70 (EN 10208-2 L 485) Provided with Simulated Corrosion (Metal Loss) Defects,” U Gent Report No. P 0173 / 0411.TL.
30. Lefevre, T., 2009, "Summary Report on Full-Scale Burst Testing of 36-inch by 12.8 mm Steel Pipes of API 5L X70 (EN 10208-2 L 485) Provided with Simulated Corrosion (Metal Loss) Defects, U Ghent Report No. P 0173 / 2402.TL.
31. PRCI EC2-5 Assess corrosion severity for high strength steels, Battelle, 2011.
32. Leis, B.N., Zhu, X.-K., and McGaughy, T., 2018, “Model Error Assessment for Pipeline Metal-Loss Defects, Phase II Report – Full-scale experiments,” PRCI Project EC-2-7, PRCI Catalog No. PR-185-143600.
33. Benjamin, A.C., Freire, J.L.F., Vieira, R.D., and Diniz, J.L.C, 2010, “Burst Tests on Pipeline Containing Circumferential Corrosion Defects,” IPC2010-31445, Proceedings of the 8th International Pipeline Conference, IPC2010, September 27-October 1, 2010, Calgary, Alberta, Canada.
34. Kim, W.S., Kim, Y.P., Kho, Y.T., and Choi, J.B., 2002, “Full Scale Burst Test and Finite Element Analysis on Corroded Gas Pipeline,” IPC2002-27037, Proceedings of the 4th International Pipeline Conference, IPC2002, September 29-October 3, 2002, Calgary, Alberta, Canada.

Appendix A Function F of Equation (10)

Bilinear interpolation for the normalized length $L/\sqrt{Dt}$ and width angle W can be used for any intermediate points. Extrapolation outside the validity range of Eq. (10) is not advised.

Table A-1 Function F in Eq. (10)

$L/\sqrt{Dt}$	W (Deg.)							
	2.5	**10.0**	**30.0**	**40.0**	**60.0**	**90.0**	**135.0**	**180.0**
0.25	0.996	0.995	0.989	0.986	0.978	0.966	0.950	0.930
0.50	0.971	0.970	0.965	0.963	0.957	0.948	0.937	0.924
0.75	0.945	0.945	0.942	0.939	0.937	0.931	0.924	0.920
1.00	0.916	0.915	0.912	0.910	0.908	0.904	0.899	0.895
1.25	0.879	0.876	0.872	0.868	0.866	0.861	0.854	0.845
1.50	0.837	0.831	0.825	0.820	0.816	0.808	0.799	0.786
1.75	0.793	0.784	0.776	0.774	0.764	0.752	0.740	0.725
2.00	0.750	0.740	0.730	0.725	0.715	0.700	0.685	0.670
2.25	0.709	0.699	0.687	0.680	0.669	0.652	0.635	0.621
2.50	0.670	0.661	0.644	0.637	0.624	0.605	0.587	0.574
2.75	0.632	0.624	0.604	0.596	0.580	0.561	0.542	0.530
3.00	0.596	0.588	0.565	0.556	0.540	0.520	0.500	0.490
3.25	0.563	0.554	0.529	0.520	0.503	0.483	0.463	0.452
3.50	0.533	0.523	0.496	0.486	0.470	0.450	0.428	0.414
3.75	0.506	0.493	0.465	0.455	0.439	0.420	0.397	0.379
4.00	0.479	0.466	0.437	0.427	0.410	0.392	0.369	0.351
4.25	0.455	0.441	0.411	0.401	0.383	0.366	0.344	0.329
4.50	0.434	0.420	0.388	0.377	0.358	0.342	0.324	0.311
4.75	0.415	0.400	0.368	0.357	0.336	0.321	0.306	0.295
5.00	0.398	0.383	0.350	0.338	0.318	0.304	0.291	0.281
5.25	0.381	0.366	0.334	0.323	0.303	0.289	0.277	0.268
5.50	0.365	0.350	0.320	0.309	0.289	0.276	0.263	0.255
5.75	0.349	0.335	0.306	0.295	0.277	0.263	0.250	0.242
6.00	0.334	0.321	0.294	0.283	0.265	0.251	0.238	0.229
6.25	0.321	0.307	0.282	0.272	0.254	0.240	0.226	0.217
6.50	0.308	0.295	0.272	0.262	0.244	0.230	0.215	0.206
6.75	0.295	0.283	0.262	0.252	0.235	0.220	0.205	0.196
7.00	0.284	0.273	0.253	0.244	0.227	0.212	0.196	0.187
7.25	0.274	0.264	0.245	0.236	0.220	0.205	0.188	0.179
7.50	0.265	0.256	0.238	0.229	0.214	0.198	0.181	0.171
7.75	0.257	0.249	0.232	0.224	0.208	0.192	0.175	0.164
8.00	0.250	0.242	0.226	0.218	0.203	0.187	0.169	0.156
8.25	0.243	0.237	0.220	0.213	0.198	0.182	0.163	0.149
8.50	0.237	0.231	0.215	0.209	0.194	0.177	0.158	0.142
8.75	0.232	0.226	0.211	0.204	0.190	0.173	0.153	0.134
9.00	0.226	0.221	0.206	0.198	0.186	0.169	0.148	0.127
9.25	0.221	0.216	0.201	0.193	0.182	0.164	0.142	0.120
9.50	0.216	0.211	0.197	0.189	0.178	0.160	0.137	0.112
9.75	0.210	0.206	0.192	0.185	0.174	0.155	0.131	0.105
10.00	0.204	0.200	0.187	0.180	0.169	0.150	0.125	0.098